

# Proposal of test experiment to evaluate performances of secondary beam mode at the high-momentum beam line

K. Shirotori<sup>1\*</sup>, K. Aoki<sup>2</sup>, W. -C. Chang<sup>3</sup>, R. Honda<sup>2</sup> T. Ishikawa<sup>4</sup>, Y. Morino<sup>2</sup>,  
M. Naruki<sup>5</sup>, H. Noumi<sup>1,2</sup>, K. Ozawa<sup>2</sup>, S. Sawada<sup>2</sup>, H. Takahashi<sup>2</sup>, and N. Tomida<sup>1</sup>

<sup>1</sup>*Research Center for Nuclear Physics (RCNP), Osaka University, Ibaraki, Osaka  
567-0047, Japan*

<sup>2</sup>*Institute of Particle and Nuclear Studies (IPNS), High Energy Accelerator  
Research Organization (KEK), Tsukuba, Ibaraki 305-0801, Japan*

<sup>3</sup>*Institute of Physics, Academia Sinica, Taipei 11529, Taiwan*

<sup>4</sup>*Research Center for Electron Photon Science (ELPH), Tohoku University, Sendai  
982-0826, Japan*

<sup>5</sup>*Graduate School of Science, Kyoto University, Kyoto 606-8502, Japan*

*ver. December 20, 2021*

## Contents

<b>1</b>	<b>Executive Summary</b>	<b>2</b>
<b>2</b>	<b>Introduction</b>	<b>3</b>
2.1	Motivation: Physics at $\pi$ 20 beam line . . . . .	3
2.2	High-momentum secondary beam line – $\pi$ 20 . . . . .	4
<b>3</b>	<b>Secondary beam mode for test experiment</b>	<b>8</b>
3.1	Modification of high-momentum beam line . . . . .	8
3.2	Background particle study . . . . .	10
3.3	Situations for test experiment . . . . .	12
3.4	Test beam line . . . . .	13
<b>4</b>	<b>Test experiment</b>	<b>14</b>
4.1	Purposes of test experiment . . . . .	14
4.2	Experimental setup . . . . .	14
<b>5</b>	<b>Beam time plan</b>	<b>19</b>
5.1	Beam time request . . . . .	19
<b>6</b>	<b>Summary</b>	<b>20</b>

---

\*Spokesperson, E-mail: [sirotori@rcnp.osaka-u.ac.jp](mailto:sirotori@rcnp.osaka-u.ac.jp)

# 1 Executive Summary

At the present hadron experimental facility, no secondary beams greater than 2 GeV/ $c$  are available. Since the J-PARC high-momentum beam line has been operated with a primary beam, the upgrade of the beam line to utilize high-momentum secondary beams,  $\pi 20$ , is strongly desired. The high-momentum beam line is designed to transport the secondary beams produced at the branching point without major modification of the beam-line configuration. Therefore, aiming to realize the  $\pi 20$  beam line, we propose a test experiment to evaluate performances of the secondary beam mode with a minimum modification of the configuration of the beam line. As the minimum modification for the test experiment, the SM collimator for the Lambertson magnet is used as a production target with a 400-watt beam loss in total along the beam line. We estimated that intensities of high-momentum secondary beams such as pions of order of  $10^5$  /spill are available with the minimum modification of the beam line configuration.

We evaluate performances of the secondary beam mode such as

- Beam intensity,
- Beam profiles (horizontal and vertical sizes with their incident angles), and
- Beam particles (pions, kaons and proton/anti-proton).

We measure momentum dependence of their performances up to 20 GeV/ $c$ . Those studies gave us important information to realize the upgrade of the beam line.

Detectors which measure delivered secondary beams are installed between the most downstream quadrupole magnet and the final focus point of the beam line. Set of beam timing detectors and scintillating fiber trackers are installed for measuring the time-of-flight of beam particles and their trajectories, respectively. For identifying secondary beam particles, a ring-imaging Cherenkov detector and threshold-type aerogel Cherenkov detectors are installed. We also use the time-of-flight method by installing timing detectors at the entrance of the experimental area and in front of the beam dump with a 20-m flight distance. We use a trigger-less data acquisition system with a streaming data-taking method for efficient data taking.

Preparations of the test experiment are supported by the hadron beam-line group of the J-PARC hadron experimental facility. The experiment will be performed after modification of the local radiation rule in order to deliver secondary beams at the J-PARC high-momentum beam line.

We request a beam time of 10 shifts (1 shift=8 hours), which can also be assigned in the commissioning by the hadron beam-line group.

<b>Beam line:</b>	High-momentum beam line
<b>Beam polarity:</b>	Negative
<b>Beam momentum:</b>	2, 3*, 5, 8, 10, 15 and 20 GeV/ $c$ (*Positive beam polarity)
<b>Beam time:</b>	3 shifts for detector commissioning, and 7 shifts for performance evaluation

## 2 Introduction

### 2.1 Motivation: Physics at $\pi 20$ beam line

Hadrons are composite particles of quarks interacting with gluons. Hence the goal of the hadron physics is to understand how quarks build hadrons. It is essential to investigate effective degrees of freedom which build the hadron structure. A quark-quark correlation, namely diquark correlation, is expected to be an effective degrees of freedom to describe baryon properties. When one quark in a baryon is replaced to a heavy quark, charm, the diquark correlation is expected to be isolated and developed in the excited states of charmed baryon [1]. As a result, two excitation modes called isotope shift such as  $\lambda$ - and  $\rho$ -modes emerge to the level structure. Excited states generated by the diquark correlation which can not be observed in light quark baryons because of the same dynamics of three diquark pairs. From the study of the excitation spectrum of charmed baryons, we can investigate the diquark correlation as an internal structure of the charmed baryons. We have already proposed a spectroscopic study of charmed baryons (J-PARC E50) [2]. In the experiment, charmed baryons ( $Y_c^{*+}$ ) are produced by the  $\pi^- p \rightarrow Y_c^{*+} D^{*-}$  reaction at the  $\pi^-$  beam momentum of 20 GeV/ $c$ . The E50 experiment needs a high-intensity pion beam at 20 GeV/ $c$  at the J-PARC high-momentum beam line.

We have proposed experiments with high-momentum secondary beams at the J-PARC high-momentum beam line. As stage-1 experiments, following experiments have been approved.

- Charmed baryon spectroscopy experiment (E50)
- Dibaryon search experiment (E79) [3]

We have also submitted a proposal and Letter of Intent (LOI) as follows.

- Spectroscopy of  $\Omega$  baryons (P85) [4]
- $\Xi$  baryon spectroscopy [5]
- Study of generalized parton distributions with exclusive Drell-Yan process [6]
- Measurement of the cross section of the  $\Lambda p$  scattering [7]
- Double anti-kaon production in nuclei by a high-momentum proton beam [8] as a related topics

High-momentum secondary beams provided by the J-PARC hadron facility are essential to investigate those hadron physics subjects. In particular, baryon spectroscopy with various flavors is vital to reveal the dynamics of effective degrees of freedom to describe baryons. The charmed baryon spectroscopy is important and closely related to the spectroscopy of multi-strangeness baryons,  $\Xi$ 's and  $\Omega$ 's. Although the spectroscopy of multi-strangeness baryons,  $\Xi$ 's and  $\Omega$ 's will be able to be performed at the K10 beam line in future, low-lying  $\Xi^*$ 's and ground state  $\Omega^-$  can be studied at the  $\pi 20$  beam line. At the present hadron experimental facility, no secondary beams greater than 2 GeV/ $c$  can be provided. Therefore, we aim to realize the  $\pi 20$  beam line to perform proposed experiments.

## 2.2 High-momentum secondary beam line – $\pi 20$

Since early 2020, the high-momentum beam line (B line) has been operated with a primary beam branched from the existing slow-extraction beam line (A line). The B line is designed to transport the secondary beams produced at the branching point in the A line without major modification of the beam-line configuration (Fig. 1), except for the most upstream part around the primary target and additional structure/equipment required for radiation safety. The beam envelope calculated by the TRANSPORT code [9] is shown in Fig. 2. The secondary beam with a negative charge produced at zero degree at the production target is departed from the primary beam course (A line) to the  $\pi 20$  beam line by using the so-called beam swinger optics [10], as illustrated in Fig. 3. For negative secondary beams, the primary beam trajectory is swung by two dipole magnets (h07 and bs0A) to the left hand side before the target and swung back by another two dipole magnets (bs0B and h13) to the A line after the target. The layout is optimized to deliver the negative secondary beams of 20 GeV/c produced at zero degree extracted to the  $\pi 20$  beam line.

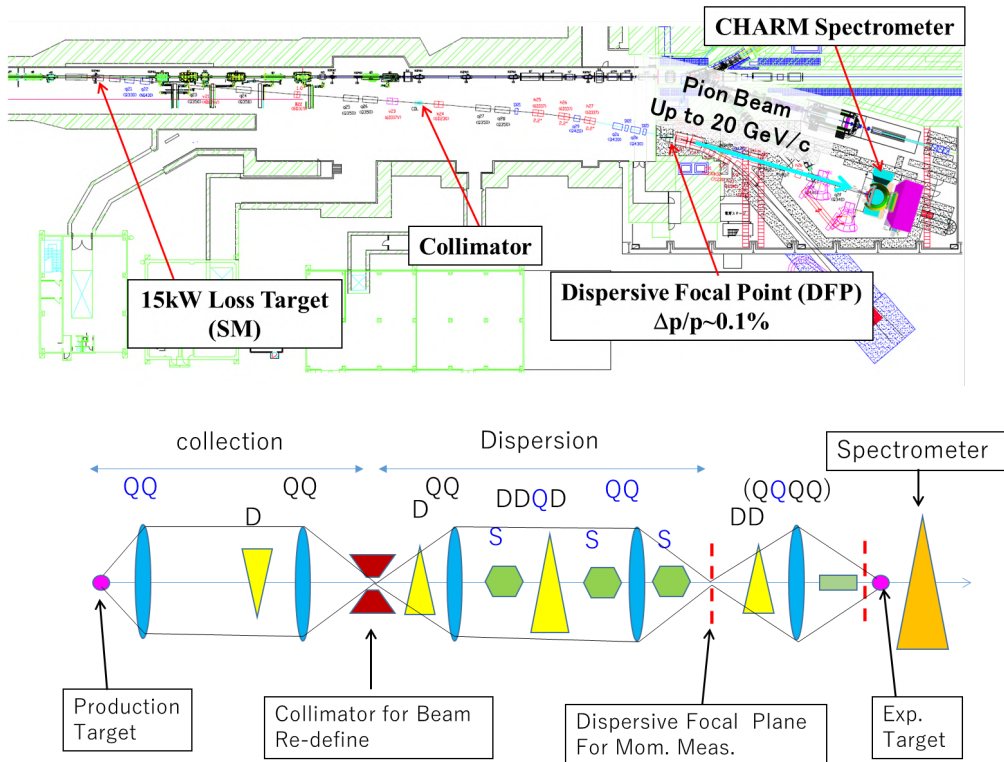


Figure 1: Plan view of the  $\pi 20$  beam line (top) and schematic illustration of the beam line configuration (bottom).

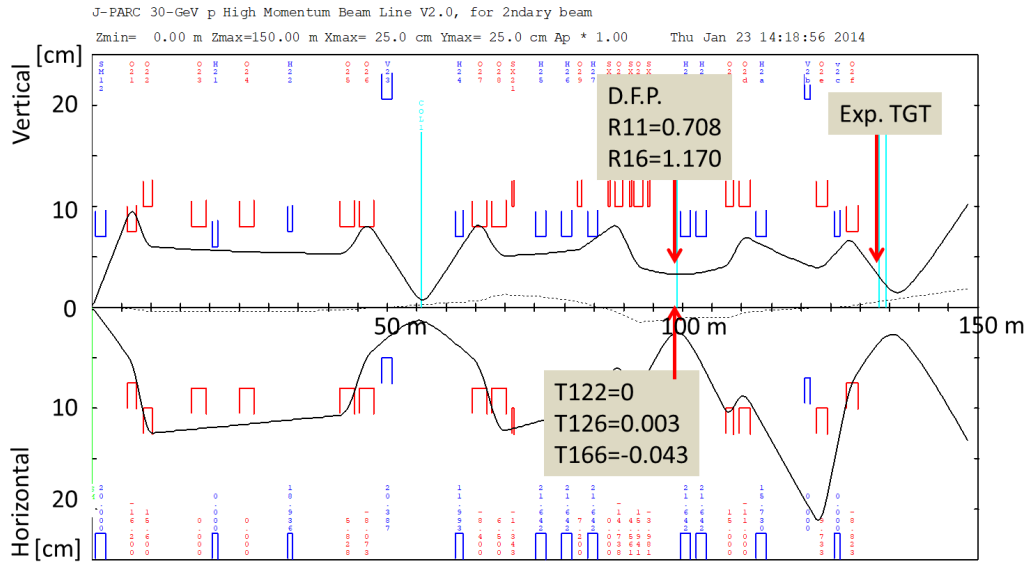


Figure 2: Beam envelope calculated by the TRANSPORT beam optics code to the second order for the  $\pi 20$  beam line.

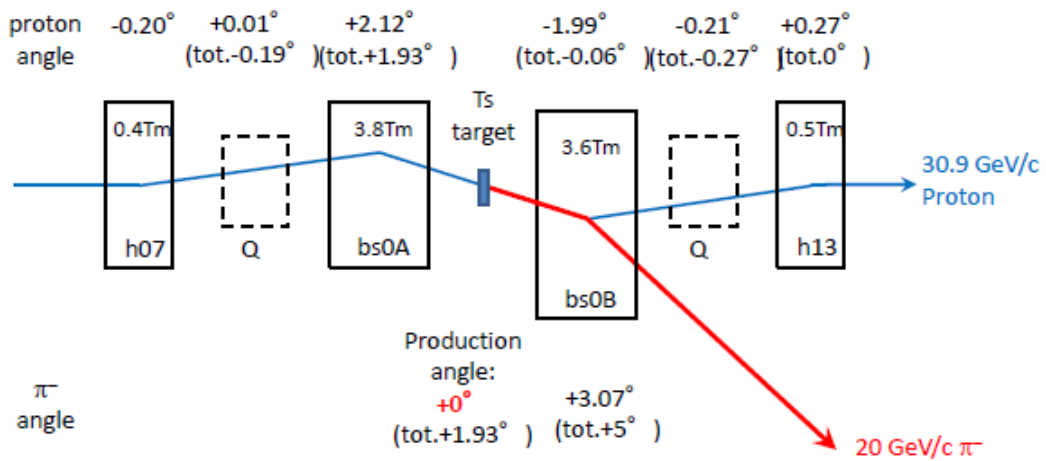


Figure 3: Proposed layout at the production target for the  $\pi 20$  beam line. For a negative secondary beam, the primary beam trajectory is swung by two dipole magnets (h07 and bs0A) to the left hand side before the target and swung back by another two dipole magnets (bs0B and h13) to the A line after the target. The layout is optimized so that the negative secondary beam of 20 GeV/c produced at zero degree is extracted to the  $\pi 20$  beam line. This is the so-called beam swinger optics [10].

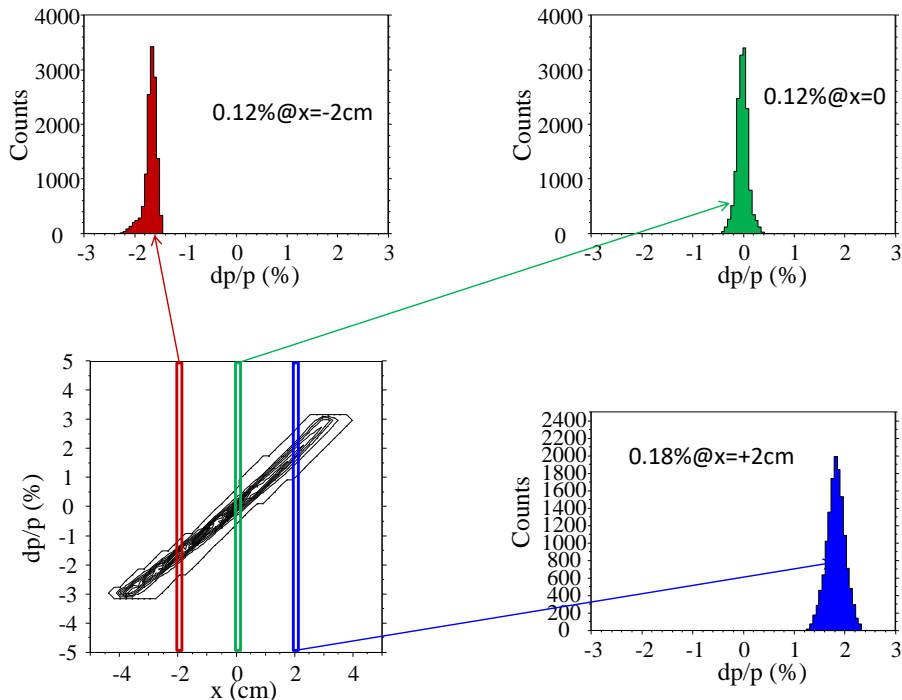


Figure 4: Correlation of horizontal position ( $x$ ) to momentum (dispersion  $dp/p(\%)$ ) of beam particles at the dispersive focal plane.

The secondary beam is collected by the first doublet of quadrupole magnets in the  $\pi 20$  beam line and focused at a collimator placed 50 m downstream from the production target to define the beam image at the production target. After the collimator, the beam is focused again at the dispersive focal plane with a large dispersion of 1.170  $\%/cm$ . Here, 4 sextupole magnets are employed to eliminate/minimize major geometric and chromatic aberrations to the second order. A correlation of horizontal position ( $x$ ) to momentum (dispersion  $dp/p(\%)$ ) of beam particles at the dispersive focal plane is calculated by TURTLE [11], as shown in Fig. 4. The figure demonstrates that a momentum resolution as good as 0.1% ( $\sigma$ ) can be realized with a spatial resolution of 1 mm for a beam particle. Beam profiles estimated by TURTLE at the experimental target is shown in Fig. 5. Figure 6 shows expected intensities of negative pions, kaons, and antiprotons per spill (5.2-second spill cycle) as functions of their momenta in the case of 30-kW primary protons on a 60-mm-long Platinum target (15-kW loss) estimated by Sangford and Wang's formula [12].

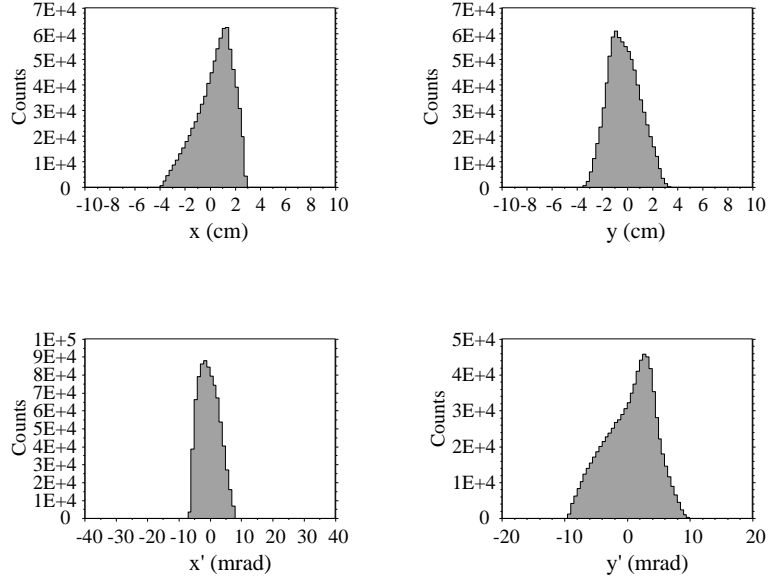


Figure 5: Beam profile estimated by TURTLE at the experimental target.

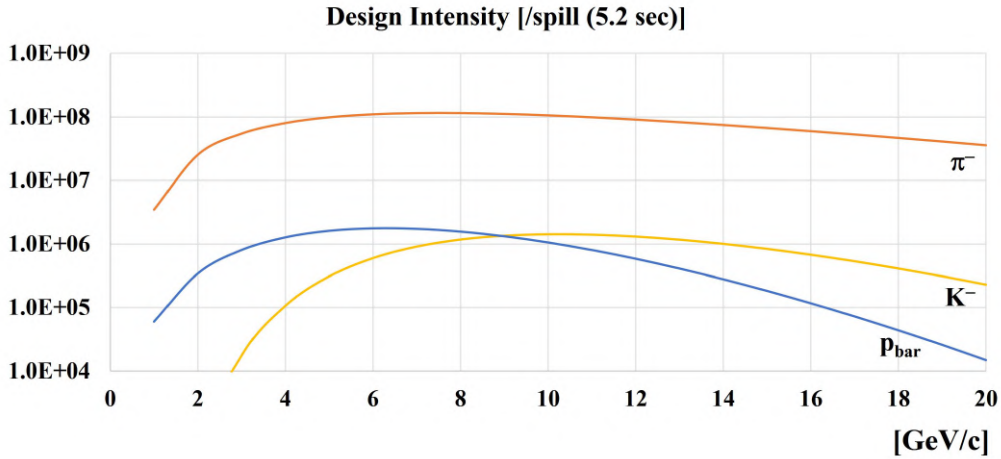


Figure 6: Expected intensities of negative pions, kaons, and antiprotons per spill (5.2-second spill cycle) as functions of their momenta in the case of 30-kW primary protons on a 60-mm-long Platinum target (15-kW loss) estimated by Sangford and Wang's formula [12].

### 3 Secondary beam mode for test experiment

For the test experiment with high-momentum secondary beams, we planned a possible minimum modification of the beam line with the support of the hadron beam-line group of the J-PARC hadron experimental facility.

#### 3.1 Modification of high-momentum beam line

As the minimum modification, we use the SM collimator for the Lambertson magnet as shown in Fig. 7(left) to produce secondary beams with a 400-watt beam loss in total along the beam line. The SM collimator consists of iron with a 340-mm length to which a part of the primary proton beam is irradiated for producing secondary beams. As shown in Fig. 7(left), the primary beam orbit is shifted to the SM collimator side. Then, the tail of the primary beam assumed reacts with the SM collimator by keeping the beam loss smaller than 400 W. Since a part of primary beam also reacts with the Lambertson magnet due to the primary beam orbit and magnet locations, the acceptable beam loss by only the SM collimator is smaller than 400 W while  $\sim 60$ -W loss occurs by the Lambertson magnet. The generated secondary beams with a scattering angle of 0.87 mrad to the vertical direction are extracted to the B line as shown in Fig. 7(right). The Lambertson magnet is not used to bend secondary beams for the extraction. At the downstream of the Lambertson magnet, there is a set of septum magnets called small (SM2) and large

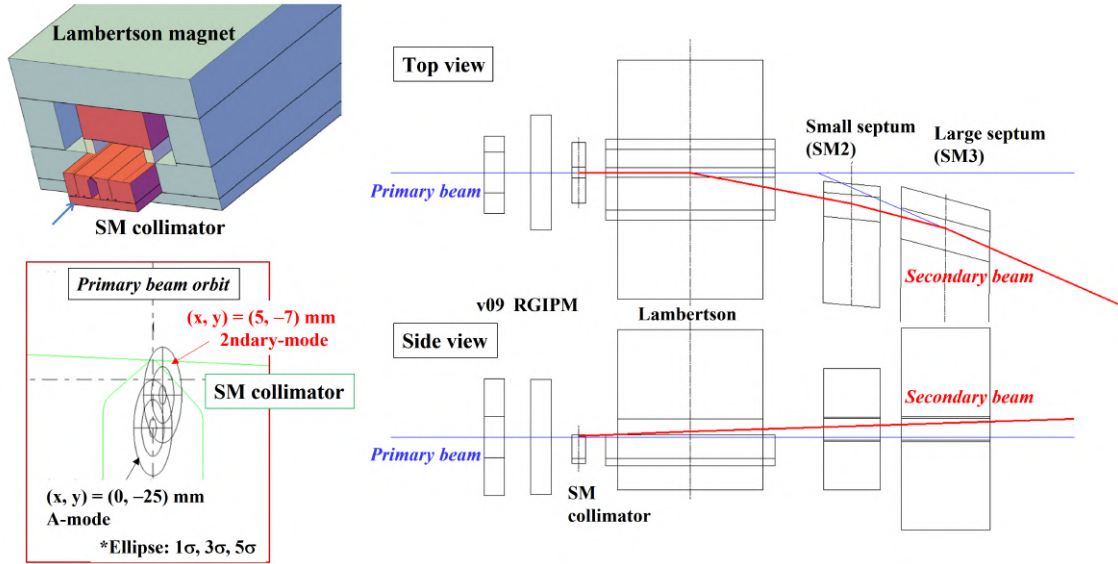


Figure 7: Schematic of the secondary beam extraction area. The schematic image of the SM collimator with the Lambertson magnet and the primary beam orbit on the SM collimator, respectively (left). The primary beam orbit is shifted to the upper side in order to react with the SM collimator. Ellipse circles show the distribution of the primary beam assumed as Gaussian. Schematic of the beam extraction magnets with the central orbit of the primary and secondary beams (right). The generated secondary beams have a scattering angle of 0.87 mrad to the vertical direction.

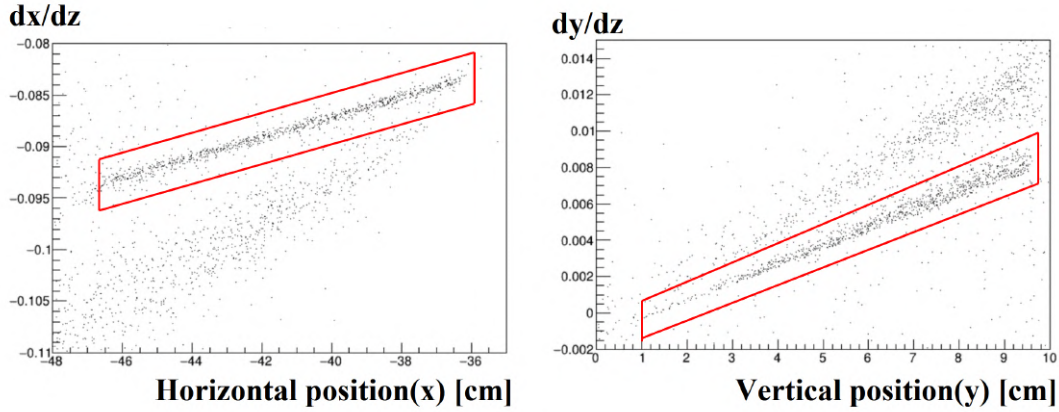


Figure 8: Correlation between incident angles along forward ( $z$  axis) direction and horizontal/vertical positions of secondary beams at the exit of the SM3 magnet. The secondary beams indicated by red square regions are accepted by the SM2 and SM3 magnets.

septum (SM3). In the case of the secondary-beam extraction, the setting of the SM2 magnet is needed to be tuned for getting a correct horizontal orbit. While the horizontal direction of the secondary beams is corrected by the SM2 magnet, the vertical one is also needed to be corrected by a vertical bending magnet called v20 which will be installed at the the downstream of the MS3 magnet. Since the generated secondary beams with a scattering angle of 0.87 mrad to the vertical direction are extracted, we need to bend secondary beams by the v20 magnet to the correct orbit by 10 mrad to the opposite vertical direction.

We simulated number of secondary beams extracted to the experimental area by using the MARS [13] and TURTLE [11] codes. Figure 8 shows correlation between incident angles along forward ( $z$  axis) direction and horizontal/vertical positions of negative pion beams at the exit of the SM3 magnet. The negative pion beams in the region indicated by red square were accepted by the SM2 and SM3 magnets. In the simulation, negative pion beams with the momentum bite of  $\pm 0.5\%$  are selected at 10 GeV/ $c$ . By simulating number of generated secondary beams with the primary proton intensity of  $50 \times 10^9$  /spill with a kinematic energy of 30 GeV by the MARS code, number of negative pion beams of  $1.1 \times 10^3$  /spill at 10 GeV/ $c$  were generated by using the tail of the primary beam with the SM colimeter. After passing through the SM3 magnet with a vertical bending by the v20 magnet, negative pion beams accepted by the B line were simulated by the TURTLE code . Figure 9 shows the beam profiles at the final focus point. The horizontal and vertical sizes and their incident angles were smaller than 2 cm and 10 mrad, respectively. From the simulation by the TURTLE code, we found that the intensity of negative pion beams of  $3.2 \times 10^2$  /spill were estimated at the final focus point. The simulation was performed with the primary proton intensity of  $50 \times 10^9$  /spill while the actual one is  $\sim 50 \times 10^{12}$  /spill so that it is found that the intensity of negative pion beams of  $\sim 3 \times 10^5$  /spill with 10 GeV/ $c$  can be delivered to the experimental area. Since the production angle of secondary beams is close to 0 degree, we can obtain the

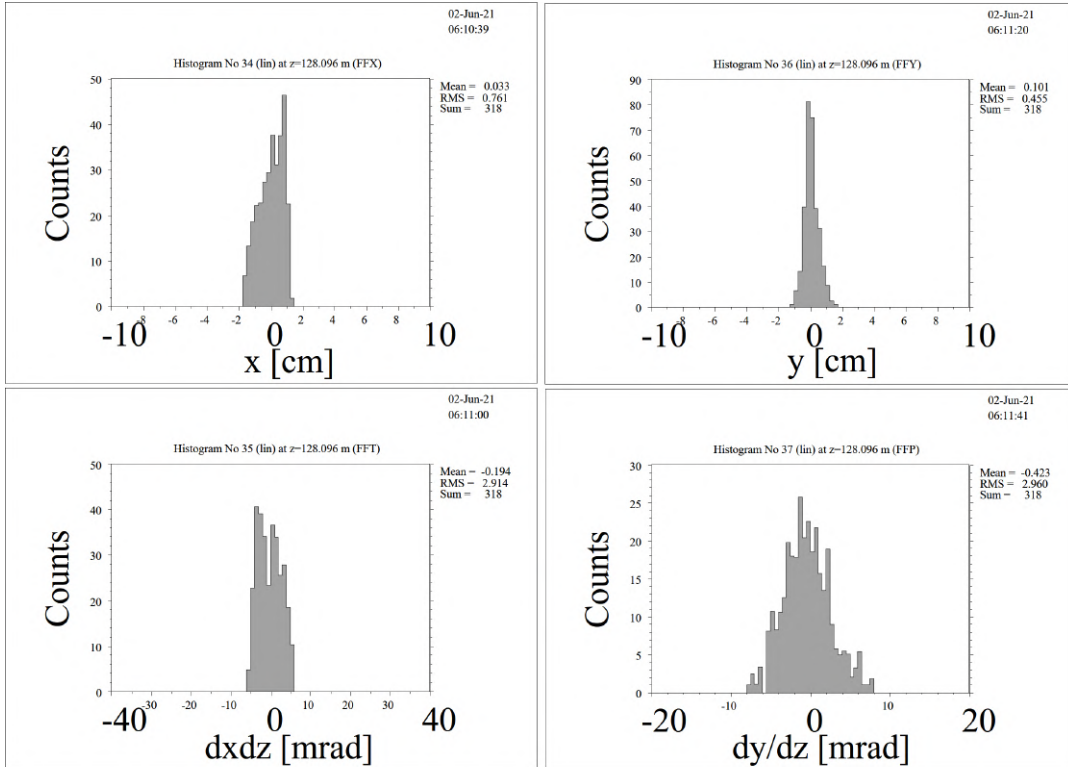


Figure 9: The beam profiles at the final focus point. Horizontal (top left) and vertical (top right) positions and their incident angles (bottom left and right for horizontal and vertical) along forward ( $z$  axis) direction.

secondary beam intensity of order of  $10^5$  /spill by the 400-W loss. The intensity of order of  $10^5$  /spill enables us to perform some experiments with high-momentum secondary beams whose major particles are positive/negative pions and proton. In addition, the momentum of secondary beams ranging from 2 to 20 GeV/ $c$  is also available because the production angle is close to 0 degree. Therefore, we found that high-momentum secondary beams up to 20 GeV/ $c$  can be utilized to perform experiments such as a pilot run of stage-1 and proposed ones by the minimum modification of the high-momentum beam line.

### 3.2 Background particle study

As a beam line study of the J-PARC high-momentum beam line we performed the measurement of the background particles in June 2021. From the study, we can evaluate the background particles produced from both SM collimator and Lambertson magnet. For surveying loss points of the primary beam, we scanned number of background particles by changing the current of the SM2 magnet. As shown in Fig. 10, we surveyed background particles from corresponding loss points at the SM collimator and the Lambertson magnet. In the measurement, the primary beam condition of the A line is the A-mode by which only A-line is used for the experiment. The conditions of the beam line optics was the same as of the E16 experimental one, except for current settings of the SM2 and the Lambertson magnet which were

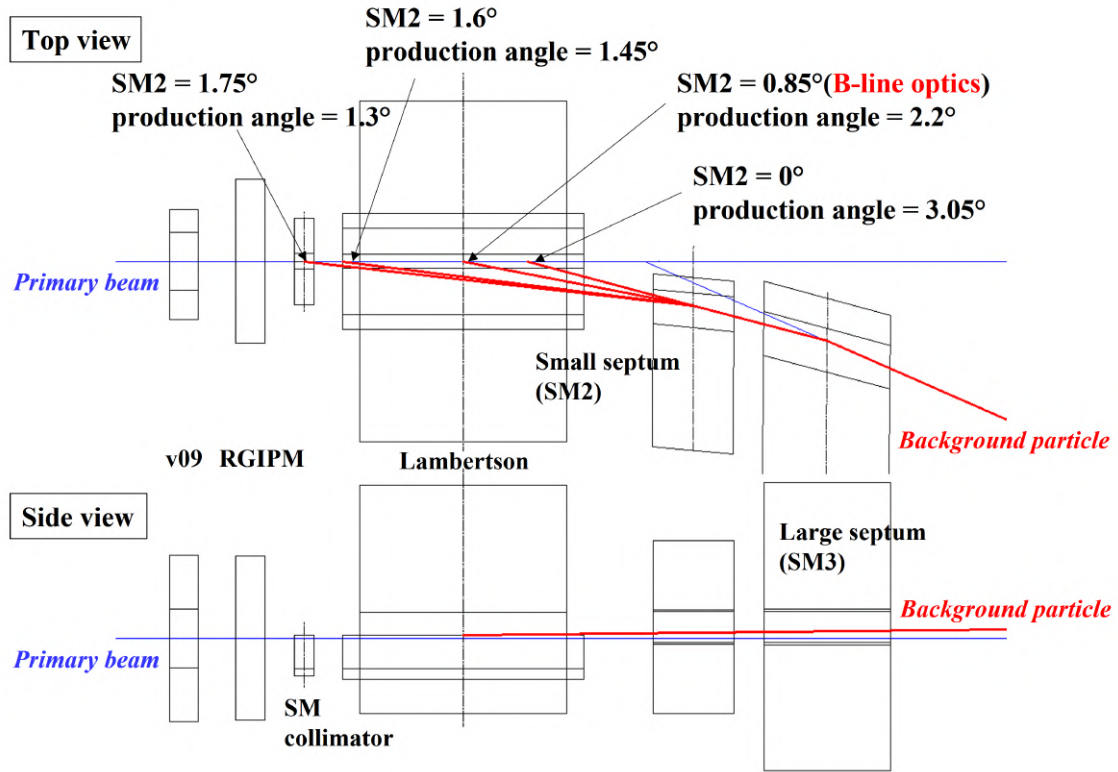


Figure 10: Corresponding loss points where background particles are produced at the SM collimator and the Lambertson magnet. Current of the SM2 magnet was scanned in order to survey loss points which produced background particles.

scanned and turned off, respectively. We scaled magnetic fields of the beam line magnet to be the 5-GeV/ $c$  condition from the 31-GeV/ $c$  one. For measuring background particles in the experimental area, we installed plastic scintillation counters with  $50 \times 50 \text{ mm}^2$  and  $70 \times 70 \text{ mm}^2$  sizes at the upstream and downstream of the E16 experimental target with a 1-m distance, respectively. Both single and coincidence rates of those counters were measured by changing the current of the SM2 magnet. Figure 11 shows the counting rates of the background particles per spill (5.2-second extraction). Around the SM collimator position which corresponds to the SM2 current of  $\sim 1200 \text{ A}$ , we found the coincidence rates of 280 counts/spill. The measured value was  $\sim 1/40$  times smaller than the expected value by the simulation because the loss of the primary beam was estimated as  $\sim 100 \text{ W}$  by the A-mode and current setting of a vertical bending magnet, called v21, was not optimized for transporting the background particles of 5 GeV/ $c$ . From the simulation, we found that the setting of the v21 magnet affected one order difference. Therefore, we could explain the order of obtained counting rates by scaling beam loss to be 400 W with a different setting of the vertical orbit by the v21 magnet. The study gave us important information to realize the upgrade of the high-momentum beam line.

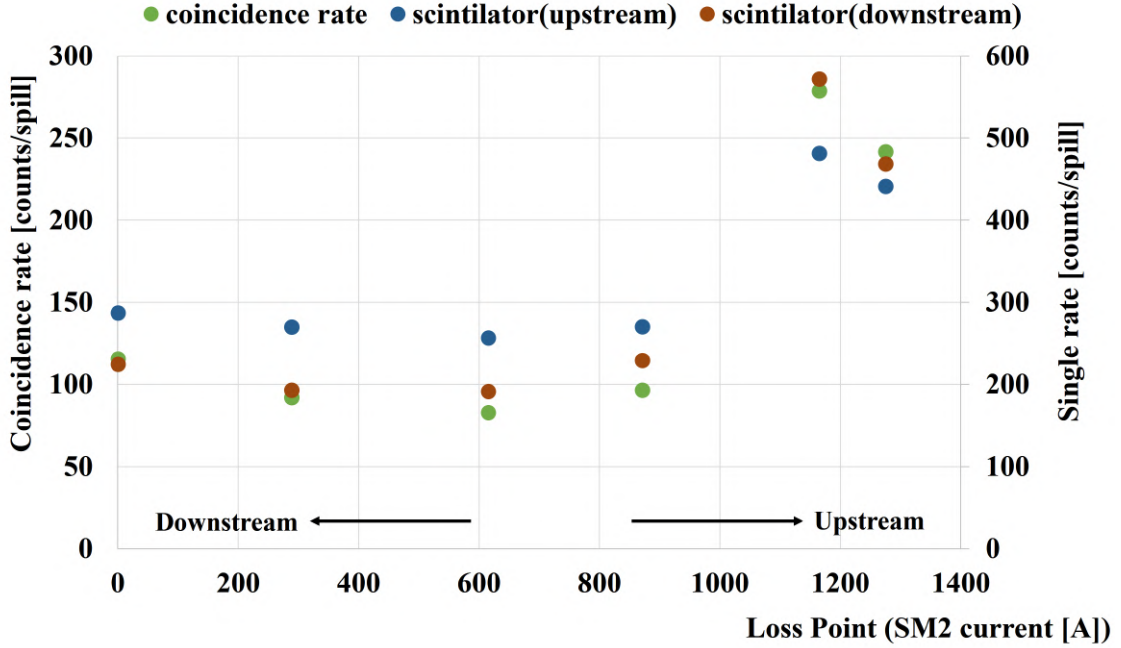


Figure 11: Counting rates of the background particles by changing the current of the SM2 magnet. The coincidence rates of 280 counts/spill around the SM collimator potions by the SM2 current of  $\sim 1200$  A.

### 3.3 Situations for test experiment

By the minimum modification to use the SM collimator as a production target, we can assume two situations to utilize high-momentum secondary beams according to the budget situation. In any cases, we will perform the test experiment to evaluate performances of the high-momentum secondary beam line.

#### Situation A

We assumed that the installations of the v20 magnet and the polarity reverse device to the power supply of the beam line magnets. In the present B line, there is no polarity reverse device so that only positive beams can be delivered to the experimental area. Polarity reverse device is necessary to utilize negative secondary beams at the high-momentum beam line. By using both v20 magnet and polarity reverse device, we can use both positive and negative beams with a beam intensity of order of  $10^5$  /spill up to 20 GeV/c to perform experiments with high-momentum secondary beams.

#### Situation B

We assumed the no installations of both v20 magnet and the polarity reverse device. In the case of the Situation B, only positive beams can be delivered to the experimental area. In addition, the vertical orbit of secondary beams is excepted to be different from the simulated one. Although the correction by the v20 magnet is necessary, acceptable profiles which enable us to perform experiments can be obtains

for tuning another vertical bending magnet called v21. We can use positive particles with a beam intensity little smaller than  $10^5$  /spill up to 20 GeV/ $c$  to perform experiments with high-momentum secondary beams. Even if there are no installations of both v20 magnet and the polarity reverse device, we aim to perform the test experiment to evaluate performances of the high-momentum secondary beam line. It is because an important milestone to realize secondary beams greater than 2 GeV/ $c$  at the J-PARC hadron experimental facility.

### **3.4 Test beam line**

After realizing to utilize the high-momentum secondary beams, we can use the high-momentum beam line not only for physics experiments but also as a test beam line for developing detectors. No test beam line which can provide high-momentum secondary beams is available in Japan. Therefore, we can expect many potential users who are developing detectors by utilizing the high-momentum secondary beams at the J-PARC hadron experimental facility.

## 4 Test experiment

### 4.1 Purposes of test experiment

We propose a test experiment to evaluate performances of the high-momentum secondary beam mode. Beam intensity, profiles, ratios of secondary beam particles and their momentum dependence up to 20 GeV/ $c$  are evaluated. Beam intensity is one of essential performances of the beam line to estimate a production yield of interested physics reactions. With the minimum modification of the beam line configuration, it is expected for secondary beams with order of  $10^5$  /spill whose intensities are measured by segmented beam timing detectors. Beam profiles at the final focus point are related to the beam line optics which determines horizontal and vertical beam sizes with their incident angles. Information of beam profiles which are measured by tracking detectors gives us the correct tuning of the beam line optics. Ratios of secondary beam particles are measured by particle identification detectors. Although positive/negative pions and proton beam intensities are dominant due to no electric separators in the beam line component, negative kaon and anti-proton intensities are important to design experiments with those secondary beams. Momentum dependence of beam intensities and ratios of secondary beams is measured by changing the beam-line momentum settings up to 20 GeV/ $c$ . Although scaled beam-line magnet current settings can be used to all beam-momentum conditions, we plan to precisely measure performances with beam momenta of 2, 3, 5, 8, 10, 15 and 20 GeV/ $c$  which are planned to be used by stage-1 and proposed experiments. Beam polarity is mainly negative while a positive polarity are used for the 3-GeV/ $c$  condition. For evaluating those performances, beam-line magnet settings are scanned by checking both beam profiles and intensity as a function of the magnet current.

### 4.2 Experimental setup

For evaluating performances of the high-momentum secondary beam mode, detectors to measure secondary beams are installed between the downstream of the final quadrupole magnet and the final focus point. For installing detectors, the present vacuum piles for the primary beam mode must be removed. All detectors are installed along the beam direction ( $z$  axis) as shown in Fig. 12. Beam intensity, profiles, ratios of secondary beam particles are measured by Cherenkov timing detectors, scintillating fiber trackers and particle identification detectors, respectively. All detectors have the active area size larger than 100 mm( $x$ ) $\times$ 100 mm( $y$ ) which is enough to measure secondary beams according to the simulation of beam profiles.

We use a trigger-less, data-streaming-type DAQ system [14] that employs fully soft-ware based event selection. In the trigger-less DAQ system, front-end electronics digitize all detector signals and continuously transfer digitized data to personal computers (PCs) without any hardware trigger. Event selection such as simple timing coincidence is performed by software on the PC. The trigger-less data-streaming-type DAQ enables us to take all beam particle data in one spill. A few spill data give us more than  $\sim 10^5$  events which are enough to evaluate performances of the high-momentum secondary beam mode.

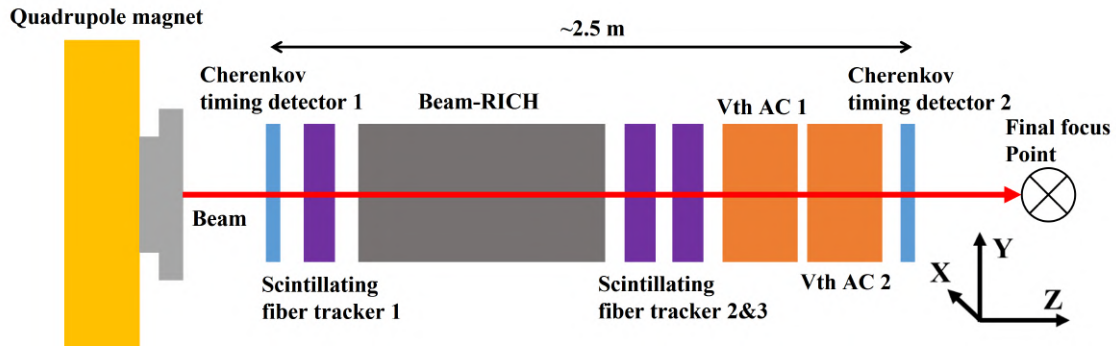


Figure 12: Schematic of experimental setup. Cherenkov timing detectors, scintillating fiber trackers, a beam-RICH detector and threshold-type aerogel Cherenkov detectors are used. All detectors are installed along the beam direction ( $z$  axis) at the downstream of the final quadrupole magnet. Flight distance between the upstream and downstream Cherenkov timing detector is  $\sim 2.5$  m.

### Timing detector: Beam timing and intensity

Set of two segmented Cherenkov timing detectors are installed to measure timing and counting rate of beam particles. The Cherenkov timing detector is made of an acrylic Cherenkov radiator that takes a cross shape (X shape) where two acrylic bars are crossed at the center [15] as shown in Fig. 13. Each bar has cross section of  $3 \times 3 \text{ mm}^2$  and a length of 150 mm. Active area of the Cherenkov timing detector with 39 bars is  $117 \text{ mm}(x) \times 105 \text{ mm}(y)$ . A multi-pixel photon counter (MPPC), Hamamatsu Photonics S13360-3050, is connected to the downstream end at each bar. The MPPCs are implemented on a shaping board with a fast operation amplifier. The shaping amplifier circuit cut the tail of the output signal from the MPPC for making the signal width narrow to  $\sim 4 \text{ ns}$  in  $\sigma$ . A timing resolution of  $\sim 40 \text{ ps}$  ( $\sigma$ ) was obtained by the test experiment [15].

Beam timing is simply measured by the time-of-flight measurement between two Cherenkov timing detectors. Although the expected beam rate is order of 100 kHz and thanks to a good timing resolution of the Cherenkov timing detector, we can neglect the accidental hits of beam particles by requiring narrow timing gate such as  $\sim 200 \text{ ps}$ . The intensity of beam particles is measured by simple timing coincidence which is performed by software on the PC.

### Tracker: Beam profiles

Beam trajectories are measured by sets of three scintillating fiber trackers. We use 9 layers in total which are installed along the  $z$  axis. The scintillating fiber tracker comprised a 0.5-mm diameter scintillating fiber, Kuraray SCSF-78M, with a staggered configuration for constructing one layer. The fibers in one layer are precisely aligned and fixed with an Epoxy-type glue. In each layer, the scintillating fibers are placed at tilt angle of  $0^\circ$ ,  $+30^\circ$  (U) and  $-30^\circ$  (V) with respect to the vertical ( $y$ ) direction. Active area of the scintillating fiber tracker is  $141 \text{ mm}(x) \times 210 \text{ mm}(y)$ . Each scintillating fiber is connected to the 1.3-mm size MPPC, Hamamatsu Photonics S13361-1350AE-08, with air contact. Figure 14 shows a photograph of the

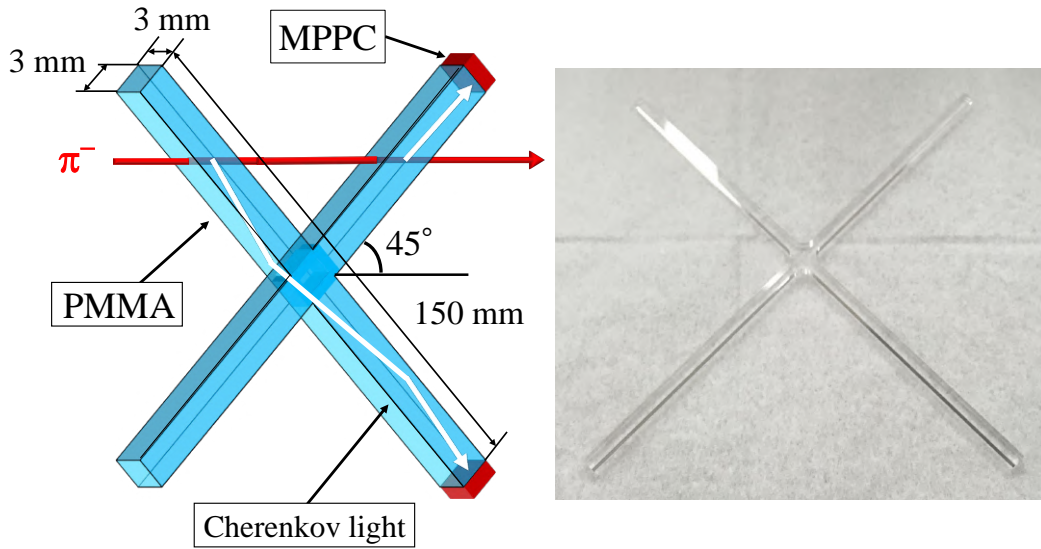


Figure 13: Schematic view (left) and photograph (right) of one segment of an X-shaped Cherenkov detector which is manufactured by carving it out of an acrylic plate. Each bar are placed at 45 degrees with respect to the beam direction. It should be noted that the emission angle of a Cherenkov light is approximately 45 degrees when high energy particles ( $\beta \sim 1$ ) passes through acrylic. We use 39 bars to the actual Cherenkov timing detector.

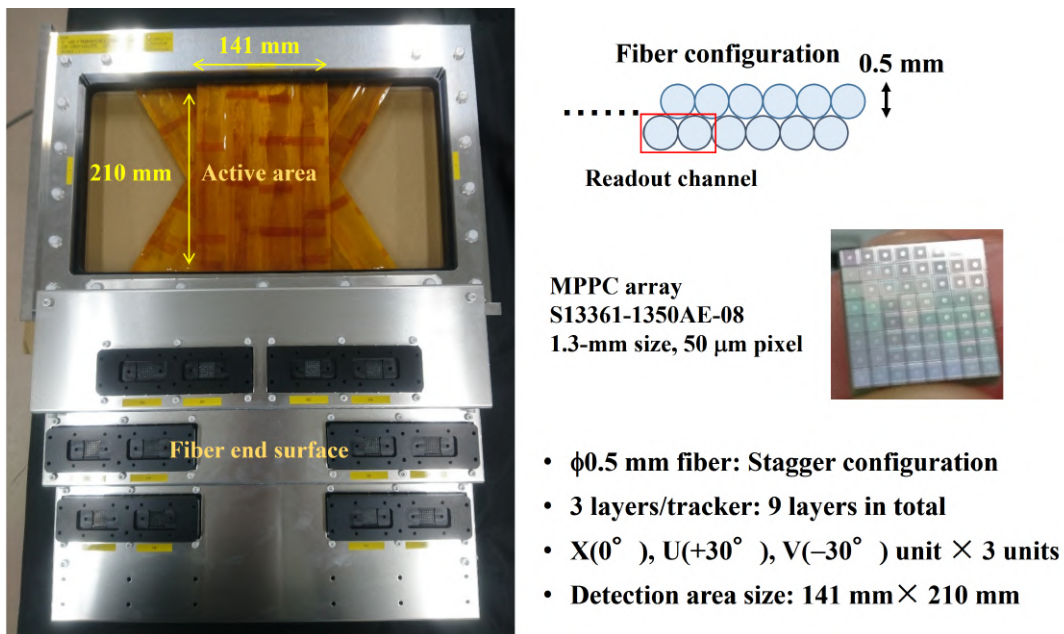


Figure 14: Photograph of the scintillating fiber tracker. Fibers are arranged to a staggered configuration for constructing one layer. 12 MPPC arrays are attached to the fiber end surfaces of the X, U, and V layers in the effective area. Two fibers are connected to one MPPC as a readout channel.

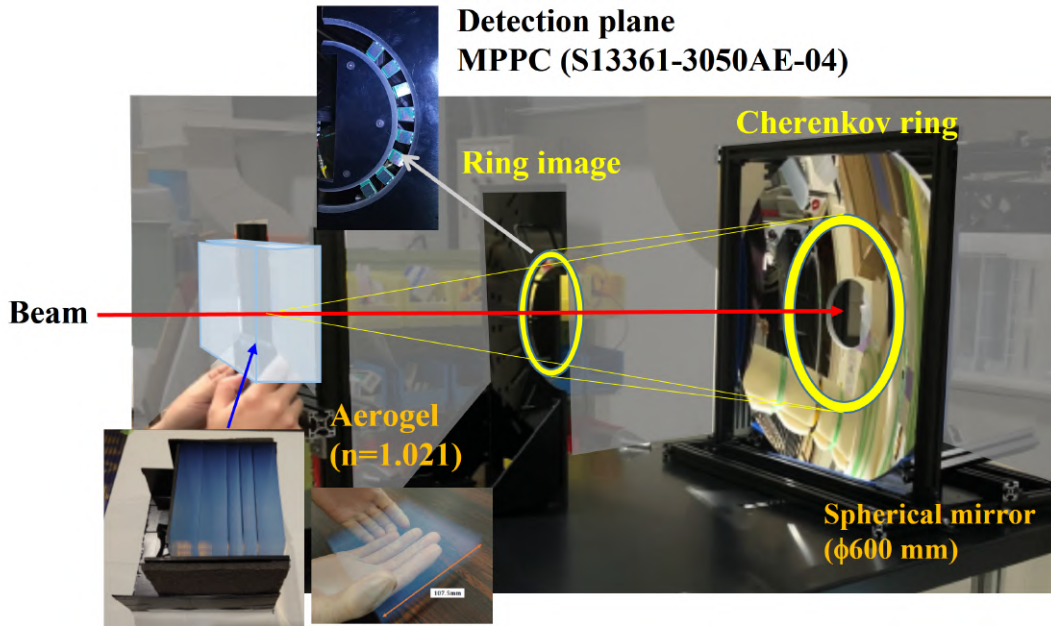


Figure 15: Photograph of the prototype bRICH detector. Silica aerogel with refractive index of 1.021 is used as a Cherenkov radiator. Cherenkov photons are once reflected at a spherical mirror and collected into MPPC arrays.

scintillating fiber tracker.

Straight tracks are found by those scintillating fiber trackers with the weight in the least square method. In finding the tracks, all combinations of hit positions on the layer were examined with a tracking routine to reduce the number of possible combinations. In the tracking routine, we obtain a 3-dimensional track with smallest  $\chi^2$  with largest number of the layer hit. Information of beam profiles at the final focus point such as horizontal (x) and vertical (y) sizes with their incident angles along the z axis ( $dx/dz$ ,  $dy/dz$ ) can be obtained.

### Particle identification detector: Beam particles

Identification of beam particles is performed by using a beam Ring-imaging Cherenkov detector (bRICH) and threshold-type Cherenkov detectors (VthAC) which can identify beam particles ranging from 5.0 to 8.5 GeV/c and from 2.0 to 4.0 GeV/c, respectively. We have developed a prototype detector of the bRICH which consists of a silica aerogel with refractive index of 1.021 as shown in Fig. 15. Cherenkov photons are once reflected at a spherical mirror and collected into MPPC arrays, Hamamatsu Photonics S13361-3050AE-04. The prototype bRICH detector shows enough performance to identify kaons and pions in the beam momentum range of 5.0 to 8.5 GeV/c [16]. VthAC detector with a silica aerogel with refractive index of 1.007 is used for identifying lower momentum particles ranging from 2.0 to 4.0 GeV/c. By combining both bRICH and VthAC, beam particles such as pions and kaon up 8.5 GeV/c can be identified. For the proton/anti-proton identification, we plan to prepare another VthACs with suitable refractive indexes. In parallel, for the particle identification up to 20 GeV/c, we are developing a RICH detector with

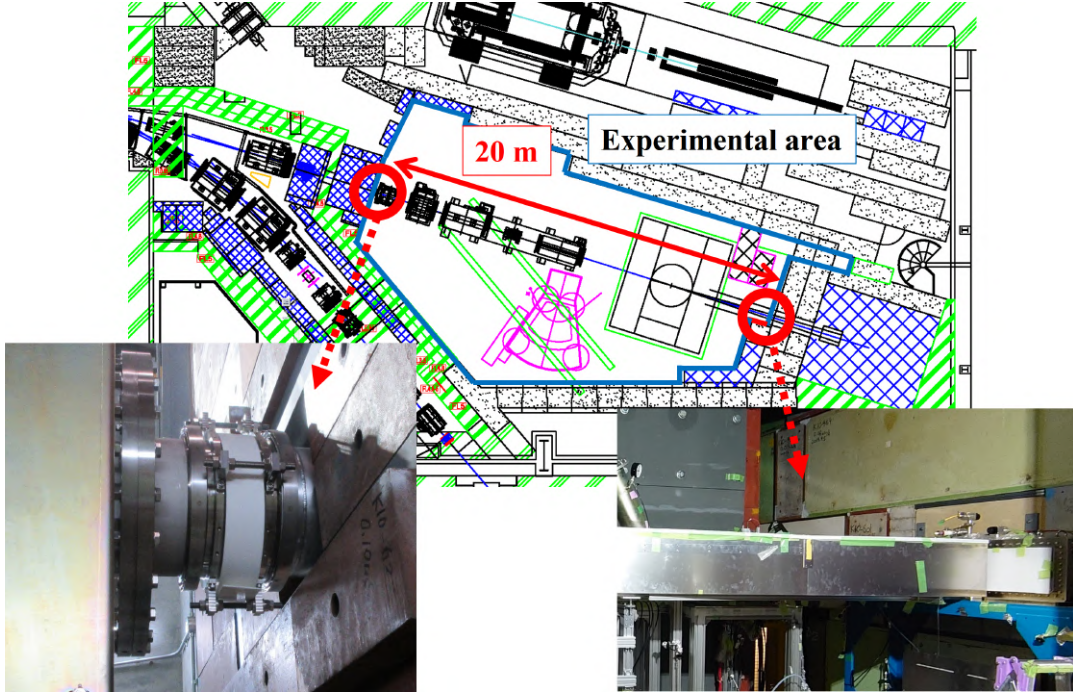


Figure 16: Schematic view of the experimental area and photographs of the entrance and in front of the beam dump. We can use a flight distance of 20 m for TOF. Beam pipes are needed to be removed in order to install timing detectors.

both silica aerogel and  $C_4F_{10}$  gas with refractive indexes of 1.04 and 1.00138, respectively. The budget for developing the RICH detector has already been secured by a Grant-in-Aid for Scientific Research [17]. We plan to install RICH to identify beam particles with their momentum up to 20 GeV/c.

### Particle identification by time-of-flight method

For redundant particle identification, we plan to also use the time-of-flight method (TOF). Due to short flight distance of  $\sim 2.5$  m between two Cherenkov timing detectors, we can only measure a coincidence event of beam particles. It is necessary to keep long flight distance by using available maximum length of the experimental area. We plan to install timing detectors at the entrance and in front of the beam dump of the experimental area as shown in Fig. 16. The flight distance of 20 m can be kept for TOF. By using the 20-m flight distance,  $\pi/K$  and  $K/\text{proton}$  with their momentum of up to 4 GeV/c and 7 GeV/c can be identified, respectively, by assuming the TOF time resolution of 100 ps( $\sigma$ ). TOF time resolution of 100 ps( $\sigma$ ) can be obtained by timing detectors with a thick plastic scintillator and a fast photomultiplier. Although only lower-momentum particles are identified by TOF, particle identifications by using three ways as bRICH, VthAC and TOF give us a confidential identification of beam particles.

## 5 Beam time plan

The experiment will be performed after modification of the local radiation rule to deliver secondary beams at the J-PARC high-momentum beam line. Preparations of the document for modifying the local radiation rule to deliver secondary beams are supported by the hadron beam-line group of the J-PARC hadron experimental facility. The earliest case of the approval of the local radiation rule is expected to be after the beginning of fiscal year of 2023. In addition, the beam time schedule of the E16 experiment using the primary beams must be considered because some modifications of the experimental area are necessary, such as removing beam piles and installing experimental apparatuses for the test experiment. Those modifications strongly affect to perform the E16 experiment so that discussions and negotiations with the E16 group are important in order to perform both experiments efficiently.

### 5.1 Beam time request

We request beam time of 10 shifts (1 shift=8 hours) by taking into account actual scheduling of the commissioning such as K1.8, K1.8BR and the high-momentum beam line with the primary beam mode. We request 3 shifts for detector commissioning and 7 shift for performance evaluation. The test experiment can be performed not only with an independent schedule but also as a part of the commissioning of the hadron beam-line group. Beam polarity is mainly negative while positive polarity is used for the 3-GeV/ $c$  condition. Even if only positive polarity is available, we also plan to perform test experiment for evaluating performances of 7 beam momenta. The following table shows the summary of the beam time request.

<b>Beam line:</b>	High-momentum beam line
<b>Beam polarity:</b>	Negative
<b>Beam momentum:</b>	2, 3*, 5, 8, 10, 15 and 20 GeV/ $c$ (*Positive beam polarity)
<b>Beam time:</b>	3 shifts for detector commissioning, and 7 shifts for performance evaluation

## 6 Summary

The upgrade of the J-PARC high-momentum beam line to utilize high-momentum secondary beams,  $\pi 20$ , is strongly desired because no secondary beams greater than 2 GeV/ $c$  are available at the present hadron experimental facility. Although the high-momentum beam line has been operated with a primary beam, the beam line is designed to transport the secondary beams produced at the branching point without major modification of the beam-line configuration. Therefore, aiming to realize the  $\pi 20$  beam line, we propose a test experiment to evaluate performances of the secondary beam mode with a minimum modification of the configuration of the beam line. As the minimum modification for the proposed test experiment, the SM collimator for the Lambertson magnet is used as a production target with a 400-watt beam loss in total along the beam line. We estimated that intensities of high-momentum secondary beams such as pions of order of  $10^5$  /spill are available with the minimum modification of the beam line configuration. Intensities of order of  $10^5$  /spill enable us to perform experiments such as pilot runs of stage-1 and proposed ones with high-momentum secondary beams.

We evaluate performances of the secondary beam mode such as beam intensity, beam profiles as horizontal and vertical sizes with their incident angles, and beam particles with their momentum dependence up to 20 GeV/ $c$ . Beam-line magnet settings are scanned by checking both beam profiles and intensity as a function of the magnet current for the evaluation. Those studies gave us important information to realize the upgrade of the high-momentum beam line.

Detectors which measure delivered secondary beams are installed between the most downstream quadrupole magnet and the final focus point of the beam line. Set of segmented Cherenkov beam timing detectors and scintillating fiber trackers are installed for measuring the time-of-flight of beam particles and their trajectories, respectively. For identifying secondary beam particles, a ring imaging Cherenkov detector and threshold-type aerogel Cherenkov detectors are installed. We also use the time-of-flight method by installing timing detectors at the entrance of the experimental area and in front of the beam dump with a 20-m flight distance. We use a trigger-less data acquisition system with a streaming data-taking method.

Preparations of the test experiment are supported by the hadron beam-line group of the J-PARC hadron experimental facility. The experiment will be performed after modification of the local radiation rule in order to deliver secondary beams at the J-PARC high-momentum beam line. Modifications of the experimental area which strongly affect to perform the E16 experiment are necessary for the secondary beam mode. We will discuss and negotiate with the E16 group in order to perform both experiments efficiently.

We request a beam time of 10 shifts, which can also be assigned in the commissioning by the hadron beam-line group. Beam polarity is mainly negative while positive polarity is used for the 3-GeV/ $c$  condition. Even if only positive polarity is available, we also plan to perform the test experiment for evaluating performances of 7 beam momenta. Evaluation of performances of the high-momentum secondary beam mode is an important milestone to realize secondary beams greater than 2 GeV/ $c$  at the J-PARC hadron experimental facility.

## References

- [1] S. H. Kim, A. Hosaka, H. C. Kim, H. Noumi, K. Shirotori, Prog. Theor. Exp. Phys. 103D01 (2014).
- [2] H. Noumi *et al.*, J-PARC Proposal E50, “Charmed Baryon Spectroscopy via the  $(\pi, D^{*-})$  reaction” (2012).
- [3] T. Ishikawa *et al.*, J-PARC Proposal E79, “Search for an I=3 dibaryon resonance” (2020).
- [4] K. Shirotori *et al.*, J-PARC Proposal P85, “Spectroscopy of Omega Baryons” (2021).
- [5] M. Naruki and K. Shirotori *et al.*, J-PARC Letter of Intent, “ $\Xi$  Baryon Spectroscopy with High-momentum Secondary Beam” (2014).
- [6] W. C. Chang *et al.*, J-PARC Letter of Intent, “Studying Generalized Parton Distributions with Exclusive Drell-Yan process at J- PARC” (2019).
- [7] R. Honda *et al.*, J-PARC Letter of Intent, “Measurement of the cross section of the  $\Lambda p$  scattering” (2020).
- [8] F. Sakuma *et al.*, J-PARC Letter of Intent, “Double Anti-kaon Production in Nuclei by Stopped Anti-proton Annihilation” (2009).
- [9] <http://aea.web.psi.ch/Urs'Rohrer/MyWeb/trans.htm>.
- [10] K. H. Tanaka, M. Ieiri, H. Noumi, M. Minakawa, Y. Yamanoi, Y. Kato, H. Ishii, Y. Suzuki, and M. Takasaki, “Optical design of beam lines at the KEK PS new experimental hall ”, Nucl. Instrum. Meth. A 363, edited by K. Ura, T. Matsuo, M. Hibino, M. Komuro, M. Kurashige, S. Kurokawa, S. Okayama, H. Shimoyama, and K. Tsuno, 114-119 (1995).
- [11] <http://aea.web.psi.ch/Urs'Rohrer/MyWeb/turtle.htm>.
- [12] J. Sanford and C. Wang, BNL internal reports Nos. 11299 and 11479 (1962).
- [13] N. V. Mokhov and O. E. Krivosheev, Fermi National Accelerator Laboratory, FERMILAB-Conf-00/181 (2000).
- [14] R. Honda *et al.*, “Continuous timing measurement using a data streaming DAQ system”, Prog. Theor. Exp. Phys., in press (2021).
- [15] T. Akaishi *et al.*, “Development of a beam-timing detector for the charmed baryon spectroscopy experiment at J-PARC”, ELPH annual report, Tohoku University 2018 (2019) 58.
- [16] M. Naruki *et al.*, “Development of RICH detector for Secondary Beam Particles at J-PARC High-momentum Beamline”, RCNP annual report, Osaka University 2020 (2020)
- [17] K. Shirotori, “Development of a particle identification detector for measuring high-momentum hadron beam reactions”, 2021-2022, Publicly Offered Research of Grant-in-Aid for scientific Research on Innovative Area (2018-2022), MEXT, Japan